HHS Public Access

Author manuscript

Brain Behav Immun. Author manuscript; available in PMC 2023 November 01.

Published in final edited form as:

Brain Behav Immun. 2022 November ; 106: 233–246. doi:10.1016/j.bbi.2022.09.001.

Neuronally expressed PDL1, not PD1, suppresses acute nociception

Kimberly A. Meerschaert[1,2,3,+], **Brian S. Edwards**[1,2,+], **Ariel Y. Epouhe**[1,2,3], **Bahiyyah Jefferson**[1,2], **Robert Friedman**[1,2], **Olivia L. Babyok**[1,3], **Jamie K. Moy**[1,2,3,+], **Faith Kehinde**[1], **Chang Liu**[4,5,+], **Creg J. Workman**[4,5], **Dario A.A. Vignali**[4,5,6], **Kathryn M. Albers**[1,2,3], **H. Richard Koerber**[1,2,3], **Michael S. Gold**[1,2,3], **Brian M. Davis**[1,2,3], **Nicole N. Scheff**[1,2,3,7], **Jami L. Saloman**[1,2,3,7,8,*]

[1]·Pittsburgh Center for Pain Research, University of Pittsburgh School of Medicine, Pittsburgh, PA

[2]·Department of Neurobiology, University of Pittsburgh School of Medicine, Pittsburgh, PA

[3]·Center for Neuroscience, University of Pittsburgh School of Medicine, Pittsburgh, PA

[4]·Department of Immunology, University of Pittsburgh School of Medicine, University of Pittsburgh, Pittsburgh, PA

[5]·Tumor Microenvironment Center, UPMC Hillman Cancer Center, Pittsburgh, PA

[6]·Cancer Immunology and Immunotherapy Program, UPMC Hillman Cancer Center, Pittsburgh, PA

[7]·Biobehavioral Cancer Control Program, UPMC Hillman Cancer Center, Pittsburgh, PA

[8]·Department of Medicine, Division of Gastroenterology, Hepatology and Nutrition, University of Pittsburgh School of Medicine, Pittsburgh, PA

Abstract

PDL1 is a protein that induces immunosuppression by binding to PD1 expressed on immune cells. In line with historical studies, we found that membrane-bound PD1 expression was largely

[*]Correspondence: Jami L. Saloman, PhD, 200 Lothrop St., Presbyterian Mezz, Department of Medicine, Division of Gastroenterology, Hepatology, and Nutrition, University of Pittsburgh, Pittsburgh, PA 15213, jls354@pitt.edu.

[+]Present Address Kimberly A. Meerschaert, Harvard University, Cambridge, MA, Brian S. Edwards, Mayo Clinic, Rochester, MN, Jamie K. Moy, Life Edit Therapeutics, Morrisville, NC, Chang Liu, Nanjing University, Nanjing, Jiangsu, China

Author Contributions

J.L.S. led the project, collected and analyzed data, and wrote the first draft of the manuscript. B.M.D and N.N.S. contributed to major revisions. K.A.M. performed retrograde labeling procedures, dissociated sensory ganglia, collected neurons and analyzed single cell qPCR data. B.S.E. performed whole ganglia and single sympathetic neuron qPCR. A.Y.E performed retrograde tracing and calcium imaging. Trigeminal neurons calcium imaging experiments and enzymatic immunohistochemistry on human DRG section were conducted by N.N.S. at New York University and University of Pittsburgh respectively. B.J. and R.F. performed single cell qPCR. J.K.M. collected and dissociated human DRG. F.K. analyzed behavioral data. O.L.B. performed behavioral experiments. C.L. and C.J.W. provided technical expertise in flow cytometry. K.M.A, M.S.G., D.A.A.V and H.R.K provided key reagents, methods and equipment. All authors contributed to data interpretation and approved the final version of the manuscript.

Declarations of Interest

JLS: Research Funding— Cygnal Therapeutics.

DAAV: cofounder and stock holder – Novasenta, Potenza, Tizona, Trishula; stock holder – Oncorus, Werewolf, Apeximmune; patents licensed and royalties - Astellas, Bristol Myers Squibb, Novasenta; scientific advisory board member - Tizona, Werewolf, F-Star, Bicara, Apeximmune; consultant - Astellas, Bristol Myers Squibb, Almirall, Incyte, G1 Therapeutics; research funding – Bristol Myers Squibb, Astellas and Novasenta.

Remaining authors have no competing interests to declare.

restricted to immune cells; PD1 was not detectable at either the mRNA or protein level in peripheral neurons using single neuron qPCR, immunolabeling and flow cytometry. However, we observed widespread expression of PDL1 in both sensory and sympathetic neurons that could have important implications for patients receiving immunotherapies targeting this pathway that include unexpected autonomic and sensory related effects. While signaling pathways downstream of PD1 are well established, little to no information is available regarding the intracellular signaling downstream of membrane-bound PDL1 (also known as reverse signaling). Here, we administered soluble PD1 to engage neuronally expressed PDL1 and found that PD1 significantly reduced nocifensive behaviors evoked by algogenic capsaicin. We used calcium imaging to examine the underlying neural mechanism of this reduction and found that exogenous PD1 diminished TRPV1-dependent calcium transients in dissociated sensory neurons. Furthermore, we observed a reduction in membrane expression of TRPV1 following administration of PD1. Exogenous PD1 had no effect on pain-related behaviors in sensory neuron specific PDL1 knockout mice. These data indicate that neuronal PDL1 activation is sufficient to modulate sensitivity to noxious stimuli and as such, may be an important homeostatic mechanism for regulating acute nociception.

Keywords

Analgesia; DRG; neuroimmune; nociceptor sensitization; reverse signaling; sex difference

1. Introduction

Neuro-immune signaling is critical for regulating homeostasis, host defense, normal nociceptive processing and pathological pain states. Sensory and sympathetic postganglionic neurons modulate the immune system via release of neurotransmitters (e.g., glutamate, norepinephrine (Gabanyi et al., 2016; Zhang et al., 2021)) and neuropeptides (e.g. CGRP (Cohen et al., 2019; Lai et al., 2020)) and in so doing, can potentiate the inflammatory response (i.e. neurogenic inflammation)(Chiu et al., 2012; Sousa-Valente and Brain, 2018). Immune cells also communicate with sensory and sympathetic neurons via secreted signals (e.g., cytokines and chemokine) that promote or inhibit nociception and pathological pain. For example, both cytokines (e.g. TNFα) and chemokines (e.g. CCL2) activate and sensitize TRPV1, an ion channel expressed by sensory neurons involved in nociception (Camprubi-Robles et al., 2009; Hensellek et al., 2007; Kao et al., 2012; Langeslag et al., 2011; Rozas et al., 2016; Utreras et al., 2013). In addition to this bidirectional paracrine signaling, recent data suggest membrane-bound, immunomodulatory proteins, specifically checkpoint proteins, contribute to neuro-immune communication (Jeon et al., 2013). Inhibitory checkpoint proteins are well known as regulators of immune homeostasis and as enablers of tumor growth through immune suppression (Hudson et al., 2020). For example, negative immune modulators such as the PDL1:PD1 pathway regulate T cell activation, cell fate, and tolerance in naïve conditions and cancer (Qin et al., 2019; Sharpe and Pauken, 2018).

The reports that *Pdcd1* (encoding PD1/CD279) may be expressed in sensory neurons generated interest in PD1 as a novel regulator of nociception in inflammatory and tumor-bearing conditions (Chen et al., 2017a; Liu et al., 2020; Shi et al., 2020; Wang et al.,

2020a; Wang et al., 2020b). Historically, PD1 had only been detected on immune and tumor cells whereas its binding partner PDL1 (encoded by *Cd274)* is expressed by several cell types, including cortical and trigeminal ganglion neurons (Jeon et al., 2013; Liu et al., 2013; Sharpe and Pauken, 2018; Shi et al., 2020). Moreover, mRNA for *Cd274*, but not *Pdcd1*, has been identified in multiple RNAseq studies of neurons in the central and peripheral nervous systems (Chiu et al., 2014; Hockley et al., 2019; Kupari et al., 2019; Usoskin et al., 2015; Wang et al., 2017; Zeisel et al., 2018). Here, we confirm the presence of PDL1 and absence of PD1 in both sympathetic postganglionic and sensory neurons and demonstrate functional consequences of intracellular PDL1 signaling *in vitro* and *in vivo*.

2. Methods

2.1 Animals

Male and female 10–12 wk C57/blk6 mice (Jackson Laboratory Stock #000664) were housed under AAALAC-accredited conditions at the University of Pittsburgh or New York University in a 12 h light/dark cycle with *ad libitum* access to water and food. Animals were cared for and studies performed in accordance with guidelines of the University of Pittsburgh or New York University Institutional Animal Care and Use Committees and the National Institutes of Health *Guide for the Care and Use of Laboratory Animals*. Where indicated, neurons were isolated from TRPV1cre:PDL1$^{fl/fl}$ mice which were generated by crossing TRPV1cre mice (Jackson Laboratory Stock #017769) with PDL1$^{fl/fl}$ mice (gift from Dr. Arlene Sharpe, Harvard University). Studies were not powered to detect sex effects, but sex was included as an independent variable in biochemical and behavioral assays. Sex was not considered for mRNA or calcium imaging due to limited sample sizes.

2.2 Human Samples

Lumbar 4 and 5 DRG from human donors were obtained with the consent of their next of kin to use their family member's tissue for research purposes. Collection and study of the DRG was approved by the University of Pittsburgh Committee for Oversight of Research and Clinical Training Involving Decedents. Consent was obtained by Center for Organ Recovery and Education staff, as was the collection of tissue. The influence of gender was not specifically considered in the analysis of study data due to limited sample size. Donor information is provided in Supplementary Table 1.

2.3 Mouse Neuron Culture

Male and female mice were anesthetized with isoflurane and transcardially perfused with cold Ca^{2+}/Mg^{2+}-free Hank's Balanced Salt Solution (HBSS, ThermoFisher Scientific, #14170161). Neuronal ganglia were dissected into cold HBSS and dissociated as described previously with the exception that neurons were resuspended in Advanced DMEM F-12 media (ThermoFisher Scientific, #12634010) containing 5% fetal bovine serum and antibiotics (penicillin/streptomycin, 50 U/ml)](Malin et al., 2007). Additionally, trigeminal ganglia neurons were further separated using a percoll gradient prior to plating. Neurons were plated on laminin/poly-d-lysine coated coverslips (Corning, cat# 431215). Neurons were allowed to adhere for 2h prior to flooding with additional media. Coverslips were used for all experiments within 8 hrs, except for transcriptional assays. For transcriptional assays,

IFNγ or vehicle was added to the neuronal media and cultures were kept overnight. IFNγ (10μg/ml stock in PBS with 0.1% bovine serum albumin (BSA)) was purchased from R & D Systems, (cat# 485-MI-100, lot# CFP2718051).

2.4 Human Neuron Culture

DRG dissociation, plating protocols and solutions used were as previously described (Zhang et al., 2015). DRG were collected from all donors within 1–2 hours after cross-clamp (time at which systemic circulation stopped). DRG were immediately placed in ice-cold collection media (in mM: 124.5 NaCl, 5 KCl, 1.2 $MgSO_4$, 1 $CaCl_2$, and 30 HEPES) pH with NaOH to 7.2 and kept on ice during travel. Upon arrival in the laboratory, DRG were transferred into fresh collection media, cleaned of connective tissue, cut into small (~1 mm^3) pieces, and enzymatically treated with 0.25% (wt/vol) collagenase P (Sigma-Aldrich, St Louis, MO), 0.15% trypsin (Worthington biochemical corporation, Lakewood, NJ), and 0.03% deoxyribonuclease I (DNAse, Worthington biochemical corporation, Lakewood, NJ) for 1.5 to 2.5 hours depending on the age of the donor. Samples were placed at 37°C with shaking at 70 RPM before mechanical dissociation using a 1mL pipette. Following mechanical dissociation, enzymatic activity was halted using 10% fetal bovine serum (FBS), 0.2% trypsin inhibitor (Sigma-Aldrich, St Louis, MO), 0.1% BSA, and 10mM $MgSO_4$. Dissociated DRG were then centrifuged at 1.7 × g for 4 min and the supernatant was removed. The remaining pellet was resuspended in 500μL of basal media, and carefully layered on top of a percoll gradient (Zhang et al., 2015) and subsequently centrifuged at 3.4 × g for 10 min. The percoll solution was removed without disturbing the pellet, neurons were resuspended in complete media and plated on poly-L-lysine coated coverslips. Neurons were allowed to adhere for at least 4h prior to flooding with additional media.

2.5 RNA Isolation and Reverse Transcription

2.5.1 Whole Ganglia—Mice were euthanized via an overdose of inhaled isoflurane and transcardially perfused with cold HBSS. Indicated tissues were dissected bilaterally and snap frozen. Bilateral ganglia were analyzed from individual mice with the exception of nodose ganglia which required pooling of two mice (total 4 ganglion) in order to isolate sufficient RNA. RNA was isolated using the Quick RNA miniprep kit (Zymo Research, Irvine, CA). RNA (0.5 μg) was reverse-transcribed using iScript cDNA synthesis kit (Bio-Rad, Hercules, CA).

2.5.2 Single Neurons—Ganglia were dissociated and plated onto coverslips as described above for human or mouse ganglia. Neurons were picked up from coverslips using borosilicate glass capillaries (World Precision Instruments, Sarasota, FL) held by a 3-axis micromanipulator, transferred to tubes containing 3μL of lysis buffer and stored at -80°C. RNA collected from each cell was reverse transcribed and amplified using T7 linear amplification (Epicentre MessageBOOSTER cDNA Synthesis kit, Lucigen) and then run through RNA Cleaner & Concentrator-5 columns (Zymo Research).

2.6 Real-time PCR

2.6.1 Primer design and validation—Primers were designed and validated as described previously (Adelman et al., 2019). Specifically for the single cell analysis, primers

were designed to fall within 500 bases of the 3' end. Primers were validated on cDNA from whole DRG. Mouse primers were also validated on universal mouse cDNA (Zyagen, San Diego, CA, cat # MD-UR-40-RH). Gel electrophoresis was used to confirm that PCR products were of predicted size without dimerization or nonspecific bands. Serial dilutions were used to calculate primer efficiencies over the range of RNA concentrations observed in single cells. Primers were accepted if efficiency was between 95% and 110%. Primer sequences can be found in Supplementary Table 2.

2.6.2 Amplification and Quantification—Sybr green PCR amplification (SsoAdvanced Universal Sybr Green Supermix, Bio-rad) was performed using a Bio-Rad CFX Connect real-time system. After amplification, a dissociation curve was plotted against the melting temperature to ensure amplification of a single product. All samples were run in duplicate. The negative control was amplification of control reaction product (product of reverse transcription of master mix in the absence of template cDNA). The relative fluorescence of SYBR green was compared with a passive reference for each cycle. Cycle time (Ct) values were determined via regression and values were recorded as a measure of initial template concentration. Quantification threshold for PCR was defined as the point at which there was a 95% replication rate (35 Ct). Relative changes (ΔCt) in mRNA levels were calculated using *Gapdh* as a reference standard and corrected for primer efficiency as previously described (Adelman et al., 2019).

2.7 Tissue Staining

2.7.1 Immunofluorescence—Mice were euthanized and perfused transcardially with 4% PFA. Human DRG were post-fixed in paraformaldehyde. All DRG were cryoprotected in 25% sucrose in 0.1 M phosphate buffer at 4°C, embedded in OCT compound (ThermoFisher Scientific, Pittsburgh, PA), sectioned (14 μm), and mounted on Superfrost Plus slides (ThermoFisher Scientific). Slides were washed, blocked in 5% normal donkey serum, 0.25% Triton and 0.1M phosphate buffer for 1 hr and then incubated in primary antibody overnight. Primary antibody information is provided in Supplementary Table 3. For PDL1 staining, tissue was subjected to additional treatment to induce de-glycosylation according to a previous publication (Lee et al., 2019). Briefly, tissue sections were exposed to denaturing buffer at 100ºC for 10 min followed by incubation with 5% PNGase F at 37ºC for 1 hr (New England Biolabs, cat# P0708). For extracellular TRPV1 staining, Triton was excluded to avoid permeabilization of cellular membranes as an extra precaution. Antibody binding was visualized with fluorophore-conjugated antibodies and details are provided in Supplementary Table 4.

2.7.2 Immunohistochemistry—Slides (4 μm sections) were deparaffinized and rehydrated using standard histological protocols. Antigen retrieval was performed using an EDTA retrieval solution and a Decloaking chamber. The secondary antibody was SignalStain Boost (HRP, Rabbit; Cell Signaling Catalog #8114, Danvers, MA).The slides were stained using an Autostainer Plus (Dako, Carpenteria, CA) platform with TBST rinse buffer (Dako). The substrate used was 3,3, Diaminobenzidine (Dako). Lastly, the slides were counterstained with Hematoxylin (Cell Signaling).

2.8 Flow Cytometry

All DRG (~54) from each mouse were collected and dissociated as described in the Mouse Neuron Culture section. Ganglia from each individual mouse was analyzed independently. The cell suspension was passed through a 105μm filter, washed and divided across a 96-well plate. Two experimental wells were created so that samples from the same mouse could be analyzed on the flow cytometer at low voltages in order to detect the large cells (ie neurons) and at high voltages to detect the significantly smaller CD45 positive cells. Several additional wells were used for a variety of positive and negative controls including unstained cells, single fluorophore staining, and 'fluorescence minus one' staining. Cells were stained with Zombie viability dye (BioLegend, San Diego, CA) for 15 min on ice. After washing, surface staining was performed for 20 min on ice. Surface markers were stained with antibodies against one or more of the following antigens: PDL1 (clone# 10F.G2; BioLegend), PD1 (clone# 29F.1A12; BioLegend), CD45.2 (clone# 104; BioLegend). Cells were then fixed in cytofix buffer (BD Biosciences) for 15 min, washed in permeabilization buffer (BD Biosciences) and stained with the intracellular neuronal marker NeuN (clone# A60; Millipore, Temecula, CA) for 45 min on ice. Data analysis was performed using FlowJo Software. Healthy live singlets were identified (~50,000 per well). Of those, NeuN (avg. ~3,000) or CD45 (avg. ~10,000) positive cells were analyzed for PDL1 or PD1 expression.

2.9 Spontaneous Nocifensive Behavior

All experiments were carried out and analyzed in a blinded manner. Intraplantar injections were made into the right hindpaw. The first injection was 15μl of vehicle (0.1% BSA in saline), active recombinant mouse PD1 (1μg, 5μg), or recombinant mouse PDL1 (1μg, 5μg). Active recombinant mouse PD1 was purchased from Abcam (ab180051) and recombinant mouse PDL1 from R&D systems (1019B7100); the stock solutions were 400μg/ml and 100μg/ml, respectively. PD1 and PDL1 were dissolved in PBS with 0.1% BSA with final working solutions containing <0.01% BSA. Concentrations of PD1 and PDL1 were chosen based on previous studies (Chen et al., 2017a). 10 min post injection, capsaicin (0.05%, 10μl) was injected intraplantar into the ipsilateral hindpaw. Capsaicin (Sigma-Aldrich, M2028) stock solution was dissolved in EtOH and diluted with sterile saline to a final concentration <0.01% EtOH. Spontaneous behavior was recorded and the 10 min period following the capsaicin injection was analyzed (Supplementary Video 1).

2.9.1 Data Analysis—The number and duration of behaviors were calculated via post-hoc analysis of the videos by a blinded observer. A second blinded observer verified the scores. Nocifensive behavior was defined as lifting, licking, biting, shaking or flinching the injected paw. Experiments were designed to be analyzed by one-way ANOVA with power of 0.80. For some experiments, secondary exploratory analyses were performed using two-way ANOVA with drug and sex as the independent variables.

2.10 Calcium Imaging

Neurons were incubated in the Ca^{2+} indicator Fura-2 AM (2 μM; ThermoFisher Scientific) with 0.02% Pluronic F-127 (Anaspec, Inc., Fremont, CA) in normal bath solution

(in mM: 130 NaCl, 5 KCl, 1.4 $CaCl_2$, 0.9 $MgCl_2$, 20 HEPES [4-(2-hydroxyethyl)-1-piperazineethanesulfonic acid], 5.5 glucose, 0.5 KH_2PO_4, 0.5 Na_2HPO_4 (pH 7.4, 320 mOsm)) containing 5 mg/mL BSA (Sigma-Aldrich, St. Louis, MO) for 30 minutes at 37°C. Coverslips were mounted on an inverted microscope stage and continuously perfused with normal bath solution. For DRG imaging, solutions were maintained at 32°C using a heated stage (Warner Instruments, Hamden, CT). For TG imaging, solutions were maintained at room temperature. Firmly attached, refractile neurons were identified as regions of interest. Fluorescence data were acquired on PC computers via CCD camera. The ratio of fluorescence emission (510nm) in response to 340/380nm excitation controlled by a Lambda filter changer (Sutter Instrument, Novato, Ca) was acquired at 1 Hz during drug application.

2.10.1 Drug Application—All drugs were applied through a computer-controlled piezo-driven perfusion system (SF-77B; Warner Instruments, Hamden, CT). Capsaicin (Sigma-Aldrich:300nM, 10mM stock) was dissolved in 1-methyl-2-pyrrolidone (1M2P) or DMSO with a final concentration <0.003% 1M2P or DMSO. Active recombinant mouse PD1 and PDL1 were prepared as described for behavior experiments. Concentrations of PD1 and PDL1 were chosen based a previous study and are reported in the text (Chen et al., 2017a).

2.10.2 Data Analysis—Data were analyzed as ΔF/Fo where $\Delta F=F_{peak}-F_o$ and F_o is the baseline fluorescence ratio. ΔF/Fo was compared across time and dose using repeated measures two-way ANOVA followed by Tukey's multiple comparisons test.

2.11 Western Blot

All DRG from two mice of the same sex were pooled and dissociated as described in section 2.3. The cell suspension plated onto two laminin coated wells of a 6-well plate. Two hours after plating, one well from each culture preparation was treated with vehicle and the other with PD1 (320ng/ml) for five minutes. Total protein was extracted on ice by homogenization in lysis buffer (Cell Signaling, cat# 9803). Protein concentration was determined via bicinchoninic acid (BCA) assay (Thermofisher Scientific). Aliquots containing 30 μg total protein were separated on SDS/PAGE gels and transferred to 0.2μm PVDF membranes using the Bio-Rad Transblot system. Nonspecific binding was blocked using 5% (wt/vol) BSA, and membranes were incubated overnight at 4°C with primary antibodies directed against p-ERK (p44/42) (1:1000; Cell Signaling, cat# 4370), total ERK (1:1000; Cell Signaling cat#9102), p-p38 (1:1000; Cell Signaling, cat# 4511), total p38 (1:1000; Cell Signaling, cat #9212) and β-tubulin III (1:5000; Sigma, cat# T2200). Protein bands were detected using donkey anti-rabbit-HRP secondary antibody (Jackson ImmunoResearch). Protein bands were visualized with Supersignal Chemiluminescent Detection reagents (Thermofisher Scientific) using an LAS3000 imager (Fujifim). Densitometry readings were calculated using the gel analyzer function in Image J software and compared via two-way ANOVA with drug and sex as the independent variables.

2.12 Quantification and analysis of membrane TRPV1

Mouse DRG cultures were prepared as described in section 2.3. Coverslips from each culture preparation were treated with 0 or 320ng/ml PD1 for 5 min. Coverslips were then fixed for 10 min with 4% PFA and immunolabeled to detect membrane bound TRPV1

(extracellular TRPV1 antibody, Alomone) without membrane permeabilization. Coverslips were photographed using the same microscope and camera settings for all images. The corrected total cell fluorescence intensity (CTCF) was determined for 20–30 neurons per coverslip per condition. The average CTCF was compared via a two-way ANOVA between groups where the independent variables were drug and genotype. For within mouse comparisons, the percent change in intensity of PD1 treated neurons versus vehicle treated neurons was also calculated and compared via student's t-test.

2.13 Quantification and statistical analysis

All statistical analyses were performed using Sigmaplot 12.0 and graphs were generated in GraphPad Prism Software. Details of specific statistical tests are found in the relevant text and figure legends. All group data are presented as mean ± SEM. A capital N is used to indicate animal and lowercase n to indicate cell number.

3. Results

3.1 *Pdcd1* and *Cd274* mRNA are expressed in whole murine sensory and sympathetic ganglia

We first assessed both *Pdcd1* and *Cd274* mRNA levels in whole neuronal ganglia using qPCR. Lymphatic tissue (pooled cervical, axial, and brachial lymph nodes (LNs)) was used as a positive control because expression of both *Pdcd1* and *Cd274* has been established in this tissue (Sharpe and Pauken, 2018). In the mouse, *Cd274* mRNA was detectable in celiac ganglia, superior cervical ganglia (SCG), nodose ganglia (NG), dorsal root ganglia (DRG, all levels) and trigeminal ganglia (TG) (Fig 1A). Expression levels of *Cd274* in sympathetic ganglia were similar to LNs, but considerably lower in sensory ganglia, as indicated by delta Ct values ($F_{(5,22)}$=8.674, p<0.001). *Pdcd1* mRNA was also detected in celiac, SCG, NG, DRG, and TG (Fig 1B). With the exception of NG, *Pdcd1* mRNA expression in these other ganglia was significantly lower than that in LNs ($F_{(5,24)}$=76.15, p<0.001).

3.2 *Cd274*, but not *Pdcd1*, mRNA is expressed in individual murine sympathetic and trigeminal ganglion neurons

Neural ganglia are comprised of multiple cell types, including satellite glia and leukocytes, both of which can express immune genes such as CD45 (Chauhan and Lokensgard, 2019; van Velzen et al., 2009). To assess neuron-specific *Pdcd1* and *Cd274* expression, murine ganglia were dissociated, plated and individual neurons were collected for single cell mRNA analysis. RNA from individual neurons was collected and analyzed by two separate laboratories that used different, independently validated primer sets (see Supplementary Table 2). Similar to published single cell RNAseq studies (Chiu et al., 2014; Hockley et al., 2019; Kupari et al., 2019; Usoskin et al., 2015; Wang et al., 2017; Zeisel et al., 2018), *Cd274* mRNA was detected in 18% of sympathetic neurons from SCG (8/44) and celiac ganglia (7/38) (Supplemental Fig 1A). *Pdcd1* mRNA was not detected in any neurons from either ganglion. Of the *Cd274*-expressing neurons, 85.7% also expressed *Npy*, a marker of sympathetic neurons (Supplemental Fig 1B). *Cd274* mRNA was detected in about half of the trigeminal sensory neurons assessed (53.3%, 8/15), while *Pdcd1* was not detected in any of these neurons (Supplemental Fig 4A).

3.3 *Cd274* is expressed in dorsal root ganglion (DRG) neurons and transcriptionally regulated by IFNγ

To characterize sensory neuron subpopulations that express *Pdcd1* and/or *Cd274*, the retrograde tracer cholera toxin subunit B conjugated to Alexa Fluor dye was injected into the skin, muscle, or visceral organs (Fig 2A). *Cd274* mRNA was detected in the majority of all DRG neurons that project to skin (100%, 13/13), muscle (91.7%, 11/12), bladder (87.5%, 14/16), colon (100%, 12/12), and pancreas (100%, 11/11) (Fig 2B). *Pdcd1* mRNA was not detected in any of these DRG neurons. Importantly, *Cd274* and *Trpv1* were co-expressed in most of the neurons screened (range: 70.8–91.7%) regardless of the tissue target, suggesting significant overlap with the nociceptive subtype of sensory neurons (Fig 2C). These data are consistent with the pattern of *Cd274* expression we reported in individual colonic afferents arising from nodose ganglia, thoracolumbar DRG, and lumbosacral DRG (Meerschaert et al., 2020).

IFNγ stimulates *Cd274* transcription in leukocytes, glia, and tumor cells (Garcia-Diaz et al., 2017). Therefore, we tested whether *Cd274* in DRG neurons was regulated by IFNγ. Using single cell mRNA analysis, we first determined that the genes encoding IFNγ receptors, *Ifngr1* and *Ifngr2*, were expressed in 94.7% (90/95) of *Cd274* positive murine DRG neurons. In central neurons, IFNγ induces transcription of other genes over 12–24hr (Bandyopadhyay et al., 1997). Over similar time periods, IFNγ (0.5–500 ng/ml) specifically drives *Cd274* transcription in nonneuronal cells (Concha-Benavente et al., 2016; Ebine et al., 2018; Garcia-Diaz et al., 2017; Numata et al., 2022; Yee et al., 2017). Based on these reports, we treated murine DRG cultures with IFNγ (0, 25, 250, 500 ng/ml) overnight before individual neurons were collected and processed for PCR analysis. IFNγ increased the amount of *Cd274* transcription in cultured sensory neurons as shown by the significant increase in the relative mRNA level compared to vehicle-treated neurons (Kruskal-Wallis: $H=32.75$, $df=3$, $p<0.001$) (Fig 2D). IFNγ treatment also increased the proportion of neurons expressing *Cd274* mRNA ($C^2_{(3)}=54.90$, $p<0.0001$) (Fig 2E).

3.4 PDL1, but not PD1 protein, is expressed in murine DRG neurons

Qualitative immunolabeling was performed on mouse DRG sections to assess the presence of PD1 and PDL1 protein (antibody information in Supplementary Tables 3 and 4). DRG sections were first immunolabeled with PGP9.5 (a pan-neuronal marker) (Fig 3A) or TRPV1 (nociceptive cation channel) (Fig 3B). After imaging, the same DRG sections were subjected to de-glycosylation treatment and immunolabeling for PDL1. PDL1 immunoreactivity was observed in both neuronal and nonneuronal cells (Fig 3A,B). Murine DRG sections from the same animals were also co-stained for PD1 and PGP9.5 (Fig 3C) or TRPV1 (Fig 3D); PD1 immunoreactivity was undetectable in neurons but was evident in nonneuronal cells.

To corroborate the immuno-localization data, protein expression of PDL1 and PD1 on dissociated murine DRG cells was quantified using flow cytometry (Fig 3E-F; Gating strategies are available in Supplementary Fig 2). The neuron-specific antibody marker, NeuN, was used to identify neuronal populations. PDL1 was detected on 60.7 ± 12.0% of NeuN positive cells, while PD1 was detected on 0.51 ± 0.2% of NeuN-positive cells (Fig 3E). In addition to immune cells, CD45 is expressed by satellite glia (van Velzen et al.,

2009, Donegan et al., 2013, Mitterreiter et al., 2017), so it was used to assess PDL1 and PD1 protein expression in nonneuronal DRG cells. Consistent with immunolabeling results, both PDL1 and PD1 were detected on nonneuronal cells via flow cytometry. Specifically, 45.56 ± 4.9% of nonneuronal CD45+ cells expressed PDL1 while 38.54 ± 4.5% expressed PD1 (Fig 3F).

3.5 Human sensory neuron expression of PD1 and PDL1

The relative level of expression of *PDCD1* and *CD274* mRNA in human DRG sensory neurons was examined in lumbar DRG from three human donors (Fig 4A; Supplementary Table 2). Ganglia were dissociated and single neurons (n=24) were collected for analysis. *CD274* mRNA was detected in 83% (20/24) of neurons assessed. In contrast to qPCR from murine sensory neurons, *PDCD1* mRNA was detected in 50% (12/24) of the neurons, albeit with high CT values (indicating less mRNA present). The relative expression level of *PDCD1* was significantly lower than that of *CD274* even when only those neurons in which detectable mRNA for both *PDCD1* and *CD274* were included in the analysis ($t_{(30)}$=3.412, p=0.002) (Fig 4B). However, these data should be interpreted with caution given the potential for contamination by satellite glia still attached to some neurons (Fig 4A).

In order to assess protein expression, human DRG sections were subjected to immunolabeling. Two independent labs conducted these studies for the purpose of validation (Saloman and Scheff). Sections were co-stained for TRPV1 as the majority of human sensory neurons express *TRPV1* mRNA (Haberberger et al., 2019). The Saloman lab performed immunofluorescent staining and observed PDL1 immunoreactivity in both neuronal and nonneuronal cells (Fig 4C). Using two different antibodies against PD1 (Biolegend (Fig 4D) and Sigma (Fig 4E)), the Saloman lab only detected PD1 immunolabeling in nonneuronal cells, putatively satellite glia. In a parallel study, the Scheff laboratory performed enzymatic immunohistochemistry on human DRG sections. The Scheff lab also detected PDL1 expression in TRPV1 positive neurons as well as in nonneuronal cells surrounding the neurons (Fig 4F). Using a third PD1 antibody (Cell Signaling), the Scheff lab detected no PD1 expression (Fig 4G).

3.6 Exogenous PD1, but not PDL1, suppresses TRPV1-dependent pain behaviors in male mice

Due to the significant overlap between *PDL1* and *TRPV1* gene expression, we examined the effects of intracellular PDL1 signaling on TRPV1-dependent nocifensive behaviors. Injection of the TRPV1 agonist capsaicin into the intraplantar region of the hindpaw is known to induce spontaneous nocifensive behaviors that include shaking, licking, biting, flinching and lifting of the injected paw (Carey et al., 2017; Hamity et al., 2010). PD1 (0, 1, or 5μg) or PDL1 (0, 1, or 5μg) was injected intraplantar (15 μl) followed by video monitoring for 10 min. Nocifensive behaviors were absent over the 10 min interval for all groups. Next, an ipsilateral intraplantar injection of capsaicin was administered (0.05% in 10μl) and the number and duration of nocifensive behaviors were assessed for the subsequent 10 min. Both the number and duration of nocifensive behaviors were assessed by a blinded experimenter. In mice receiving a prior injection of PD1, the number of capsaicin-

evoked nocifensive behaviors was reduced compared to vehicle-treated mice ($F_{(2,21)}$=4.971, p=0.017) (Fig 5A; Supplementary Video 1). The duration of capsaicin-evoked behaviors was also reduced by PD1 pretreatment ($F_{(2,20)}$=5.064, p=0.017) (Fig 5B). This study was designed to detect significant drug effects with a power of 0.80, and significant differences were detected between groups. However, the power was only 0.65. While not originally powered to detect an influence of sex, exploratory analyses were performed to determine whether a sex effect might contribute to the decrease in power detected with the one-way ANOVA. Unexpectedly, differences between males and females were large enough to detect an interaction between sex and drug with a two-way ANOVA (power >0.89). There were significant main effects of both sex and drug (sex: $F_{(1,18)}$=14.723, p=0.001; drug: $F_{(2,18)}$=8.244, p=0.003) (Fig 5C). The effect of sex appeared to be due to a PD1-induced suppression of capsaicin-evoked behavior in males not detected in females. Comparable results were obtained with a two-way ANOVA of the duration of capsaicin-evoked behavior data, where there was a trend toward a significant interaction between sex and drug, (sex*drug: $F_{(2,17)}$=3.02, p=0.075) (Fig 5D). Unexpectedly, pretreatment with a high dose of recombinant PDL1 resulted in an increase in the number of capsaicin-evoked nocifensive behaviors ($F_{(2,30)}$=3.999, p=0.029) (Fig 5E). An exploratory two-way ANOVA revealed a main effect of sex (p=0.02) and drug (p=0.014) (Fig 5F). However, there was no effect of PDL1 on the overall duration of capsaicin-evoked behaviors (Fig 5G,H). Given that some mice engaged in a single behavior such as lifting for extended uninterrupted periods, the small but significant increase in the number of nocifensive behaviors should not be overinterpreted. To determine if neuronally expressed PDL1 is necessary for the inhibitory effects of exogenous PD1, we assessed capsaicin-evoked behaviors in TRPV1cre:$PDL1^{fl/fl}$ mice in which PDL1 is not expressed in sensory neurons. Pretreatment with PD1 reduced the number of capsaicin-evoked nocifensive behaviors in genotype controls but had no impact in TRPV1cre:$PDL1^{fl/fl}$ mice (genotype*drug: $F_{(2,35)}$=4.489, p=0.018) (Fig 5I). Similarly, administration of PD1 reduced the duration of capsaicin-evoked nocifensive behaviors in genotype controls but had no effect in the knockout mice (genotype*drug: $F_{(2,35)}$=5.22, p=0.01) (Fig 5J).

3.7 PDL1, but not PD1, signaling suppresses acute TRPV1-dependent nociception

To determine whether the PD1:PDL1-induced changes in nocifensive behaviors were due to the direct effect of drug on TRPV1 signaling in sensory neurons, we performed *in vitro* Fura2-AM based calcium imaging. Capsaicin was applied three times (300nM, 4s) to dissociated DRG neurons, with a minimum inter-stimulus interval of 10 min to minimize tachyphylaxis (Fig 6A, blue vehicle trace). After the first capsaicin-evoked response returned to baseline (minimum 5 min), vehicle (<0.01% BSA) or PD1 (32ng/ml, 320ng/ml) was applied for 5 min. There was no change in intracellular Ca^{2+} in response to PD1 alone (Fig 6A, green trace). However, pretreatment with 32ng/ml PD1 significantly inhibited the second capsaicin-evoked response (defined as ≥15% decrease in the second response compared to the first transient) in 32 out of 37 neurons tested (Fig 6B, Supplementary Fig 3B). There was no measurable recovery in response to a third application of capsaicin in 9 out of 32 neurons that met the criterion for a PD1-induced suppression of the capsaicin-evoked transient (Supplementary Figure 3B). In DRG cultures treated with 320ng/ml PD1, 41 out 50 neurons exhibited a suppression of the second capsaicin-evoked transient;

20 out of 41 neurons did not exhibit recovery in response to the third application of capsaicin (Supplementary Fig 3C). The Scheff laboratory independently investigated the effects of PDL1 signaling in dissociated trigeminal ganglia neurons where 15 out of 16 neurons exhibited a PD1-induced suppression of the transient and subsequent recovery (Supplementary Fig 4).

Using the same experimental paradigm, we assessed the effects of soluble PDL1 (0, 1, or 10 ng/ml) on wild-type DRG neurons. PDL1 had no significant effect on capsaicin responses (Fig 6C,D; Supplementary Fig 3D-F)). In order to confirm that the effects of extracellular PD1 require neuronal PDL1, we examined capsaicin-evoked calcium transients in neurons isolated from TRPV1cre:PDL1$^{fl/fl}$ mice (Fig 6E). PD1 reduced the proportion of capsaicin responders in control neurons, but not PDL1 knockout neurons (two-way ANOVA: genotype*drug: $F(2,12)=6.904$, $p=0.01$) (Fig 6F). These observations suggest that PD1 binding to afferent-expressed PDL1 underlies the suppression of capsaicin evoked transients.

3.8 PDL1-dependent suppression of TRPV1 is independent from changes in p-ERK or p-p38

In non-neuronal PDL1 expressing cells, binding of PD1 to PDL1 has been shown to regulate intracellular ERK and p38 kinases (Black et al., 2016; Wu et al., 2018). Activation, via phosphorylation, of ERK and p38 can drive transcription and activation of other kinases and phosphatases (Reffas and Schlegel, 2000; Wortzel and Seger, 2011; Zheng et al., 2011). Activation of both ERK and p38 have been implicated in the regulation of TRPV1 activity (Ji et al., 2002; Zhu and Oxford, 2007). Based on these results, we hypothesized that a downregulation of phosphorylated ERK (p-ERK) or phosphorylated p38 (p-p38) could underlie the PDL1-mediated suppression of capsaicin responses observed in male mice. To determine if PDL1-dependent modulation of these kinases occurs in DRG neurons, cultures were treated with PD1 (0 or 320ng/ml) for 5 min followed by immunoblotting to measure p-p38 and p-ERK. Under naïve conditions, DRG cultures derived from female mice expressed significantly higher levels of p-p38 compared to cultures derived from male mice (two-way ANOVA: Sex: $F_{(1,14)}=10.07$, $p=0.007$), but treatment with PD1 had no effect on the level of p-p38 (Supplementary Fig 5A,B). On the other hand, PD1 induced a significant sex specific increase in p-ERK which was due to an increase in p-ERK in cultures derived from female, but not male mice (two-way ANOVA: sex*drug: $F_{(1,21)}=14.64$, $p=0.001$) (Supplementary Fig 5E,F). There were no significant differences in the relative expression levels of total p38 (Supplementary Fig 5C,D) or total ERK (Supplementary Fig 5G,H). These data do not support our hypothesis and suggest that PDL1-dependent suppression of TRPV1 is independent from changes in p-ERK or p-p38.

3.9 Engaging neuronal PDL1 decreases membrane TRPV1

Another mechanism that could explain how PDL1 activation leads to suppression of capsaicin-induced nocifensive behavior and alterations in calcium signaling is that PD1-binding to PDL1 modulates expression or conductance of membrane bound TRPV1. To test this possibility, DRG cultures from either TRPV1cre:PDL1$^{fl/fl}$ or control littermates were prepared in the same manner as described in section 2.3. Coverslips generated from both genotypes were treated with 0 or 320ng/ml for 5 min followed by immunolabeling

with a TRPV1 antibody targeting an extracellular domain (Fig 7A). Application of PD1 significantly reduced membrane TRPV1 in control neurons but had no effect on neurons from TRPV1cre:PDL1$^{fl/fl}$ mice (two-way ANOVA followed by Sidak test: drug*genotype: $F_{(1,15)}$=10.15, p=0.006) (Fig 7B). To allow for within animal comparisons, coverslips from a single mouse were used for both vehicle and drug treatments. The TRPV1 fluorescent signal was 46% lower in PD1-treated control neurons compared to vehicle-treated neurons derived from the same mouse ($t_{(7)}$=3.208, p=0.004) (Fig 7C). These data indicate that intracellular signaling downstream of PDL1 causes internalization or removal of membrane bound TRPV1, providing a potential mechanism for the changes in behavior and calcium transients following activation of neuronal PDL1.

4. Discussion

Here we refine expression data and extend knowledge of the functional role for PD1:PDL1 signaling in nociceptive primary sensory afferents. We have shown *Cd274* mRNA is widespread in both somatic and visceral afferents and a subpopulation of post-ganglionic sympathetic neurons. We also demonstrated that *Cd274* mRNA was detected in 83% of human sensory neurons. Using single nucleus RNAseq (snRNAseq) to probe human DRG neurons, Traveres-Ferreira and colleagues also detected widespread *CD274* (in all neuron RNA clusters) (Tavares-Ferreira et al., 2021). We also visualized PDL1 protein in both human and mouse spinal sensory neurons and confirmed localization by flow cytometry of dissociated mouse DRG neurons. Expression of PDL1 on spinal sensory neurons is consistent with earlier studies reporting PDL1 expression in murine trigeminal sensory neurons (Jeon et al., 2013; Shi et al., 2020).

Pdcd1 mRNA expression in mouse and human sensory neurons has also been reported (Chen et al., 2017a; Liu et al., 2020; Shi et al., 2020; Wang et al., 2020a; Wang et al., 2020b). However, three independent laboratories contributing to the present study were unable to detect neuronal *Pdcd1* mRNA and/or protein in mouse neurons. It should be noted that previous mouse single cell RNAseq studies also reported no *Pdcd1* mRNA in sensory or sympathetic neurons (Chiu et al., 2014; Hockley et al., 2019; Kupari et al., 2019; Usoskin et al., 2015; Wang et al., 2017; Zeisel et al., 2018). Moreover, we were unable to reproduce the results from the original study that examined PD1 in sensory neurons (Chen et al., 2017a), despite using the same PD1 antibody (Fig 3, 4); our immunolabeling and flow cytometry analyses indicated that only non-neuronal cells in mouse were immunoreactive for PD1. The presence of PD1 in non-neuronal cells could account for several conclusions from the original study in which functional studies were done on whole, partially digested ganglia that included satellite cells as well as different populations of immune cells (Chen et al., 2017a). While PD1 (mRNA or protein) was undetectable in mouse neurons in the present study, we did detect low levels of *PDCD1* mRNA in human sensory neurons. Nevertheless, our DRG culture and immunofluorescence labeling suggests that at least some of the signal may have originated from adherent satellite cells, which are difficult to separate from adult human DRG neurons in the acute setting (Fig 4A), requiring at least 24 hours in culture to fully detach from neurons. A new snRNAseq study on human DRG also did not detect *PDCD1* (personal communication, Steve Davidson). However, it should be noted

that the Travares-Ferreira et al snRNAseq did detect *PDCD1*, albeit at particularly low levels (Tavares-Ferreira et al., 2021).

In the present study, exogenous PD1 induced no spontaneous behavior in the 10 min following intraplantar injection. There was a significant reduction in capsaicin-evoked nocifensive behaviors in male mice, suggesting that neuronal PD1-evoked PDL1 intracellular signaling is anti-nociceptive. There are several examples of sex differences in pain along the neuraxis (Presto et al., 2022). Other anti-nociceptive molecules (e.g. delta opioid agonists) are significantly more potent in males (Saloman et al., 2011), so it is possible that if we tested higher concentrations of PD1 a similar effect would be observed in females. None of our analyses revealed marked differences in PDL1 expression that would explain the lack of efficacy in female mice. Moreover, we observed PDL1-dependent suppression of TRPV1 Ca^{2+} flux in neurons derived from both male and female DRG. However, Mapplebeck and colleagues' review of sex differences in neuroimmune regulation of pain, points out that while microglia proliferate in the spinal cord in both sexes following peripheral nerve injury, they only induce upregulation of the P2X4 receptor in males (Mapplebeck et al., 2016). Thus, differences in the signaling mechanisms downstream of PDL1 may explain the behavioral differences in male and female mice following treatment with exogenous PD1. Additional studies are needed to more thoroughly investigate the mechanisms responsible for the observed sex difference.

In contrast to our data, Chen and colleagues administered the same concentration of PD1 (5 μg) under naïve conditions and observed a significant decrease in mechanical threshold suggesting a pro-nociceptive effect (Chen et al., 2017a). The underlying reason for the inconsistency between our findings and theirs is unclear. One possibility is differences in the structure of soluble PD1 that was used. Soluble (not membrane-bound) PD1 and PDL1 splice variants have been identified in humans; soluble PD1 and PDL1 lack the transmembrane domain but contain the extracellular Ig domains and maintain the ability to bind PDL1 and PD1, respectively (Sharpe and Pauken, 2018; Zhu and Lang, 2017). In the current study, we used active recombinant mouse PD1 containing the extracellular domain mimicking endogenous soluble PD1, whereas Chen and colleagues used a disulfide-linked homodimer in which the extracellular domain was fused with human IgG1.

We observed an increase in the number of capsaicin-evoked nocifensive behaviors following administration of 5 μg PDL1 that appears to be due to a selective effect in females. While this suggests the possibility that extraneuronal PDL1 is pronociceptive in females, we are cautious not to overinterpret the data, particularly given that there was no difference in the duration of behaviors or any other parameter examined. For example, we observed no changes in capsaicin-evoked calcium transients following pretreatment with PDL1 in neurons collected from female mice. At the very least, this implies that any behavioral effects of exogenous PDL1 are not due to a direct action on neurons which is consistent with our data indicating that the binding partner, PD1, is not expressed on the neurons. Elevated levels of soluble PDL1 have been detected in patients with acute pancreatitis (Chen et al., 2017b), an inflammatory condition in which pain is a diagnostic criterion. This observation is consistent with the possibility that PDL1 is pro-nociceptive, but through an indirect pathway. In our study, the exogenous PDL1 could be driving nociception by binding to PD1,

putatively expressed on resident and infiltrating immune cells. This would prevent PD1 from being able to bind to the neuronal PDL1, resulting in the loss of PDL1-dependent neuron inhibition thereby promoting nociception and pain.

In the current study, application of PD1 was associated with increased phosphorylation of ERK1/2 in DRG cultures from female mice. Neuronal p-ERK is thought to be pro-nociceptive, potentiating TRPV1 via increased transcription, translation and phosphorylation (Camprubi-Robles et al., 2009; Hensellek et al., 2007; Kao et al., 2012; Langeslag et al., 2011; Rozas et al., 2016; Utreras et al., 2013). If PD1 binding to PDL1 induces p-ERK in female neurons it could theoretically potentiate TRPV1 or at least counteract PDL1-dependent internalization of membrane-bound TRPV1. This could explain why there was no apparent PD1-induced suppression of capsaicin-evoked behavior in female mice.

We suggest the actions of PD1 observed in the present study are the result of PDL1 signaling in sensory afferents given that the effects are absent in TRPV1cre:PDL1$^{fl/fl}$ mice. Little is known about the intracellular signaling downstream of PDL1 because the primary focus in immunology has been on the PD1-expressing cells. However, we do know that PD1 binding to PDL1 inhibits dendritic cell activity, as measured by increased IL-10 that limits the pro-inflammatory activity of the cells (Kuipers et al., 2006). Similarly, we observed a reduction in TRPV1 calcium signaling following application of PD1 suggesting that PD1 binding to PDL1 has an inhibitory effect on sensory neurons, suppressing nociception and pain behavior. Given the lack of data regarding signaling cascades downstream of PDL1, we based our initial hypothesis on two studies in nonneuronal cells (dendritic and tumor) showing that PDL1 signaling regulates p-ERK and p-p38 (Black et al., 2016; Jalali et al., 2019; Wu et al., 2018), which are known for modulating transcription and downstream kinase and phosphatase activity. However, we saw no difference in p-ERK or p-p38 in male DRG, suggesting that PDL1-dependent suppression of TRPV1 signaling does not require changes in p-ERK or p-p38. Given the short time period (5–10 minutes) in which PDL1 has its antinociceptive effect, other likely explanations include loss of membrane bound TRPV1. This is supported by our data showing that exogenous PD1 blocks TRPV1 calcium flux and reduces the relative levels of TRPV1 immunoreactivity in the membrane. Future studies will be needed to further investigate the processes mediating membrane expression of TRPV1 which could range from local translation (Tohda et al., 2001) to changes in receptor internalization (Camprubi-Robles et al., 2009; Sanz-Salvador et al., 2012).

Checkpoint proteins like PDL1 play an important role in balancing immunopathology and protective immunity, homeostasis and tolerance (Qin et al., 2019). Many cell types of finite lifespan (e.g. endothelial and epithelial cells) express PDL1 as a means of maintaining tolerance and preventing autoimmunity (Sharpe and Pauken, 2018). Sensory and post-ganglionic sympathetic neurons are post-mitotic, making their axons exposed continuously to the immune system for the life of the animal, resulting in an even greater need to induce immune tolerance. The ability of PD1 to attenuate TRPV1 signaling is consistent with this idea; neuron-immune communication that decreases sensitivity of afferent neurons would also decrease peripheral release of molecules known to drive inflammation and potentially damage peripheral neuron processes. Thus, expression of a checkpoint protein like PDL1

could be an effective mechanism for afferent neurons to limit their exposure to a cytotoxic environment produced by active immune cells.

Supplementary Material

Refer to Web version on PubMed Central for supplementary material.

Acknowledgements

This work was supported by T32 NS073548 (KAM, BSE, JKM, JLS), Hirshberg Foundation (JLS), Hillman Cancer Center (BMD, DAAV, JLS), P01 AI108545 (DAAV) and UG3 TR003090 (MSG). This project also used the UPMC Hillman Cancer Center and Tissue and Research Pathology/Pitt Biospecimen Core shared resource that is supported in part by award P30CA047904. The authors thank Christopher Sullivan for maintaining the mouse colony as well as Dr. Emanuel Loeza-Alcocer and Vidhya Nagarajan for assistance with human DRG dissociation and Isabella Babyok for additional behavioral analyses. The authors acknowledge the Center for Organ Recovery and Education (CORE) for their help in coordinating receipt of tissue from organ donors. The authors also thank the donor family members for graciously consenting to the use of their loved ones' tissue for research purposes.

References

Adelman PC, Baumbauer KM, Friedman R, Shah M, Wright M, Young E, Jankowski MP, Albers KM, Koerber HR, 2019. Single-cell q-PCR derived expression profiles of identified sensory neurons. Mol Pain 15, 1744806919884496.

Bandyopadhyay A, Chakder S, Rattan S, 1997. Regulation of inducible and neuronal nitric oxide synthase gene expression by interferon-gamma and VIP. Am J Physiol 272, C1790–1797.

Black M, Barsoum IB, Truesdell P, Cotechini T, Macdonald-Goodfellow SK, Petroff M, Siemens DR, Koti M, Craig AW, Graham CH, 2016. Activation of the PD-1/PD-L1 immune checkpoint confers tumor cell chemoresistance associated with increased metastasis. Oncotarget 7, 10557–10567.

Camprubi-Robles M, Planells-Cases R, Ferrer-Montiel A, 2009. Differential contribution of SNARE-dependent exocytosis to inflammatory potentiation of TRPV1 in nociceptors. FASEB J 23, 3722–3733. [PubMed: 19584302]

Carey LM, Gutierrez T, Deng L, Lee WH, Mackie K, Hohmann AG, 2017. Inflammatory and Neuropathic Nociception is Preserved in GPR55 Knockout Mice. Sci Rep 7, 944. [PubMed: 28428628]

Chauhan P, Lokensgard JR, 2019. Glial Cell Expression of PD-L1. Int J Mol Sci 20.

Chen G, Kim YH, Li H, Luo H, Liu DL, Zhang ZJ, Lay M, Chang W, Zhang YQ, Ji RR, 2017a. PD-L1 inhibits acute and chronic pain by suppressing nociceptive neuron activity via PD-1. Nat Neurosci.

Chen Y, Li M, Liu J, Pan T, Zhou T, Liu Z, Tan R, Wang X, Tian L, Chen E, Qu H, 2017b. sPD-L1 Expression is Associated with Immunosuppression and Infectious Complications in Patients with Acute Pancreatitis. Scand J Immunol 86, 100–106. [PubMed: 28513984]

Chiu IM, Barrett LB, Williams EK, Strochlic DE, Lee S, Weyer AD, Lou S, Bryman GS, Roberson DP, Ghasemlou N, Piccoli C, Ahat E, Wang V, Cobos EJ, Stucky CL, Ma Q, Liberles SD, Woolf CJ, 2014. Transcriptional profiling at whole population and single cell levels reveals somatosensory neuron molecular diversity. Elife 3.

Chiu IM, von Hehn CA, Woolf CJ, 2012. Neurogenic inflammation and the peripheral nervous system in host defense and immunopathology. Nat Neurosci 15, 1063–1067. [PubMed: 22837035]

Cohen JA, Edwards TN, Liu AW, Hirai T, Jones MR, Wu J, Li Y, Zhang S, Ho J, Davis BM, Albers KM, Kaplan DH, 2019. Cutaneous TRPV1(+) Neurons Trigger Protective Innate Type 17 Anticipatory Immunity. Cell 178, 919–932 e914.

Concha-Benavente F, Srivastava RM, Trivedi S, Lei Y, Chandran U, Seethala RR, Freeman GJ, Ferris RL, 2016. Identification of the Cell-Intrinsic and -Extrinsic Pathways Downstream of EGFR and IFNgamma That Induce PD-L1 Expression in Head and Neck Cancer. Cancer Res 76, 1031–1043. [PubMed: 26676749]

Ebine K, Kumar K, Pham TN, Shields MA, Collier KA, Shang M, DeCant BT, Urrutia R, Hwang RF, Grimaldo S, Principe DR, Grippo PJ, Bentrem DJ, Munshi HG, 2018. Interplay between interferon regulatory factor 1 and BRD4 in the regulation of PD-L1 in pancreatic stellate cells. Sci Rep 8, 13225.

Gabanyi I, Muller PA, Feighery L, Oliveira TY, Costa-Pinto FA, Mucida D, 2016. Neuro-immune Interactions Drive Tissue Programming in Intestinal Macrophages. Cell 164, 378–391. [PubMed: 26777404]

Garcia-Diaz A, Shin DS, Moreno BH, Saco J, Escuin-Ordinas H, Rodriguez GA, Zaretsky JM, Sun L, Hugo W, Wang X, Parisi G, Saus CP, Torrejon DY, Graeber TG, Comin-Anduix B, Hu-Lieskovan S, Damoiseaux R, Lo RS, Ribas A, 2017. Interferon Receptor Signaling Pathways Regulating PD-L1 and PD-L2 Expression. Cell Rep 19, 1189–1201. [PubMed: 28494868]

Haberberger RV, Barry C, Dominguez N, Matusica D, 2019. Human Dorsal Root Ganglia. Frontiers in Cellular Neuroscience 13.

Hamity MV, White SR, Hammond DL, 2010. Effects of neurokinin-1 receptor agonism and antagonism in the rostral ventromedial medulla of rats with acute or persistent inflammatory nociception. Neuroscience 165, 902–913. [PubMed: 19892001]

Hensellek S, Brell P, Schaible HG, Brauer R, Segond von Banchet G, 2007. The cytokine TNFalpha increases the proportion of DRG neurones expressing the TRPV1 receptor via the TNFR1 receptor and ERK activation. Mol Cell Neurosci 36, 381–391. [PubMed: 17851089]

Hockley JRF, Taylor TS, Callejo G, Wilbrey AL, Gutteridge A, Bach K, Winchester WJ, Bulmer DC, McMurray G, Smith ESJ, 2019. Single-cell RNAseq reveals seven classes of colonic sensory neuron. Gut 68, 633–644. [PubMed: 29483303]

Hudson K, Cross N, Jordan-Mahy N, Leyland R, 2020. The Extrinsic and Intrinsic Roles of PD-L1 and Its Receptor PD-1: Implications for Immunotherapy Treatment. Front Immunol 11, 568931.

Jalali S, Price-Troska T, Bothun C, Villasboas J, Kim HJ, Yang ZZ, Novak AJ, Dong H, Ansell SM, 2019. Reverse signaling via PD-L1 supports malignant cell growth and survival in classical Hodgkin lymphoma. Blood Cancer J 9, 22. [PubMed: 30783096]

Jeon S, St Leger AJ, Cherpes TL, Sheridan BS, Hendricks RL, 2013. PD-L1/B7-H1 regulates the survival but not the function of CD8+ T cells in herpes simplex virus type 1 latently infected trigeminal ganglia. J Immunol 190, 6277–6286. [PubMed: 23656736]

Ji RR, Samad TA, Jin SX, Schmoll R, Woolf CJ, 2002. p38 MAPK activation by NGF in primary sensory neurons after inflammation increases TRPV1 levels and maintains heat hyperalgesia. Neuron 36, 57–68. [PubMed: 12367506]

Kao DJ, Li AH, Chen JC, Luo RS, Chen YL, Lu JC, Wang HL, 2012. CC chemokine ligand 2 upregulates the current density and expression of TRPV1 channels and Nav1.8 sodium channels in dorsal root ganglion neurons. J Neuroinflammation 9, 189. [PubMed: 22870919]

Kuipers H, Muskens F, Willart M, Hijdra D, van Assema FB, Coyle AJ, Hoogsteden HC, Lambrecht BN, 2006. Contribution of the PD-1 ligands/PD-1 signaling pathway to dendritic cell-mediated CD4+ T cell activation. Eur J Immunol 36, 2472–2482. [PubMed: 16917960]

Kupari J, Haring M, Agirre E, Castelo-Branco G, Ernfors P, 2019. An Atlas of Vagal Sensory Neurons and Their Molecular Specialization. Cell Rep 27, 2508–2523 e2504.

Lai NY, Musser MA, Pinho-Ribeiro FA, Baral P, Jacobson A, Ma P, Potts DE, Chen Z, Paik D, Soualhi S, Yan Y, Misra A, Goldstein K, Lagomarsino VN, Nordstrom A, Sivanathan KN, Wallrapp A, Kuchroo VK, Nowarski R, Starnbach MN, Shi H, Surana NK, An D, Wu C, Huh JR, Rao M, Chiu IM, 2020. Gut-Innervating Nociceptor Neurons Regulate Peyer's Patch Microfold Cells and SFB Levels to Mediate Salmonella Host Defense. Cell 180, 33–49 e22.

Langeslag M, Constantin CE, Andratsch M, Quarta S, Mair N, Kress M, 2011. Oncostatin M induces heat hypersensitivity by gp130-dependent sensitization of TRPV1 in sensory neurons. Mol Pain 7, 102. [PubMed: 22196363]

Lee HH, Wang YN, Xia W, Chen CH, Rau KM, Ye L, Wei Y, Chou CK, Wang SC, Yan M, Tu CY, Hsia TC, Chiang SF, Chao KSC, Wistuba II, Hsu JL, Hortobagyi GN, Hung MC, 2019. Removal of N-Linked Glycosylation Enhances PD-L1 Detection and Predicts Anti-PD-1/PD-L1 Therapeutic Efficacy. Cancer Cell 36, 168–178 e164.

Liu BL, Cao QL, Zhao X, Liu HZ, Zhang YQ, 2020. Inhibition of TRPV1 by SHP-1 in nociceptive primary sensory neurons is critical in PD-L1 analgesia. JCI Insight 5.

Liu Y, Carlsson R, Ambjorn M, Hasan M, Badn W, Darabi A, Siesjo P, Issazadeh-Navikas S, 2013. PD-L1 expression by neurons nearby tumors indicates better prognosis in glioblastoma patients. J Neurosci 33, 14231–14245.

Malin SA, B.M D, Molliver DC, 2007. Production of dissociated sensory neuron cultures and considerations for their use in studying neuronal function and plasticity. Nature Protocols 2, 152–160. [PubMed: 17401349]

Mapplebeck JCS, Beggs S, Salter MW, 2016. Sex differences in pain: a tale of two immune cells. Pain 157 Suppl 1, S2–S6. [PubMed: 26785152]

Meerschaert KA, Adelman PC, Friedman RL, Albers KM, Koerber HR, Davis BM, 2020. Unique Molecular Characteristics of Visceral Afferents Arising from Different Levels of the Neuraxis: Location of Afferent Somata Predicts Function and Stimulus Detection Modalities. J Neurosci 40, 7216–7228. [PubMed: 32817244]

Numata Y, Akutsu N, Ishigami K, Koide H, Wagatsuma K, Motoya M, Sasaki S, Nakase H, 2022. Synergistic effect of IFN-gamma and IL-1beta on PD-L1 expression in hepatocellular carcinoma. Biochem Biophys Rep 30, 101270.

Presto P, Mazzitelli M, Junell R, Griffin Z, Neugebauer V, 2022. Sex differences in pain along the neuraxis. Neuropharmacology 210, 109030.

Qin W, Hu L, Zhang X, Jiang S, Li J, Zhang Z, Wang X, 2019. The Diverse Function of PD-1/PD-L Pathway Beyond Cancer. Front Immunol 10, 2298. [PubMed: 31636634]

Reffas S, Schlegel W, 2000. Compartment-specific regulation of extracellular signal-regulated kinase (ERK) and c-Jun N-terminal kinase (JNK) mitogen-activated protein kinases (MAPKs) by ERK-dependent and non-ERK-dependent inductions of MAPK phosphatase (MKP)-3 and MKP-1 in differentiating P19 cells. Biochem J 352 Pt 3, 701–708. [PubMed: 11104676]

Rozas P, Lazcano P, Pina R, Cho A, Terse A, Pertusa M, Madrid R, Gonzalez-Billault C, Kulkarni AB, Utreras E, 2016. Targeted overexpression of tumor necrosis factor-alpha increases cyclin-dependent kinase 5 activity and TRPV1-dependent Ca2+ influx in trigeminal neurons. Pain 157, 1346–1362. [PubMed: 26894912]

Saloman JL, Niu KY, Ro JY, 2011. Activation of peripheral delta-opioid receptors leads to anti-hyperalgesic responses in the masseter muscle of male and female rats. Neuroscience 190, 379–385. [PubMed: 21664434]

Sharpe AH, Pauken KE, 2018. The diverse functions of the PD1 inhibitory pathway. Nat Rev Immunol 18, 153–167. [PubMed: 28990585]

Shi S, Han Y, Wang D, Guo P, Wang J, Ren T, Wang W, 2020. PD-L1 and PD-1 expressed in trigeminal ganglia may inhibit pain in an acute migraine model. Cephalalgia 40, 288–298. [PubMed: 31640402]

Sousa-Valente J, Brain SD, 2018. A historical perspective on the role of sensory nerves in neurogenic inflammation. Seminars in Immunopathology 40, 229–236. [PubMed: 29616309]

Tavares-Ferreira D, Shiers S, Ray PR, Wangzhou A, Jeevakumar V, Sankaranarayanan I, Chamessian A, Copits BA, Dougherty PM, Gereau RW, Burton MD, Dussor G, Price TJ, 2021. Spatial transcriptomics reveals unique molecular fingerprints of human nociceptors. bioRxiv, 2021.2002.2006.430065.

Usoskin D, Furlan A, Islam S, Abdo H, Lonnerberg P, Lou D, Hjerling-Leffler J, Haeggstrom J, Kharchenko O, Kharchenko PV, Linnarsson S, Ernfors P, 2015. Unbiased classification of sensory neuron types by large-scale single-cell RNA sequencing. Nat Neurosci 18, 145–153. [PubMed: 25420068]

Utreras E, Prochazkova M, Terse A, Gross J, Keller J, Iadarola MJ, Kulkarni AB, 2013. TGF-beta1 sensitizes TRPV1 through Cdk5 signaling in odontoblast-like cells. Mol Pain 9, 24. [PubMed: 23668392]

van Velzen M, Laman JD, Kleinjan A, Poot A, Osterhaus AD, Verjans GM, 2009. Neuron-interacting satellite glial cells in human trigeminal ganglia have an APC phenotype. J Immunol 183, 2456–2461. [PubMed: 19635905]

Wang J, Kollarik M, Ru F, Sun H, McNeil B, Dong X, Stephens G, Korolevich S, Brohawn P, Kolbeck R, Undem B, 2017. Distinct and common expression of receptors for inflammatory mediators in vagal nodose versus jugular capsaicin-sensitive/TRPV1-positive neurons detected by low input RNA sequencing. PLoS One 12, e0185985.

Wang K, Gu Y, Liao Y, Bang S, Donnelly CR, Chen O, Tao X, Mirando AJ, Hilton MJ, Ji RR, 2020a. PD-1 blockade inhibits osteoclast formation and murine bone cancer pain. J Clin Invest 130, 3603–3620. [PubMed: 32484460]

Wang Z, Jiang C, He Q, Matsuda M, Han Q, Wang K, Bang S, Ding H, Ko MC, Ji RR, 2020b. Anti-PD-1 treatment impairs opioid antinociception in rodents and nonhuman primates. Sci Transl Med 12.

Wortzel I, Seger R, 2011. The ERK Cascade: Distinct Functions within Various Subcellular Organelles. Genes Cancer 2, 195–209. [PubMed: 21779493]

Wu X, Li Y, Liu X, Cao S, Harrington SM, Chen C, Mansfiled AS, Dronca RS, Park SS, Yan Y, Kwon L, Ling K, Dong H, 2018. B7-H1(PD-L1) confers chemoresistance through ERK and p38 MAPK pathway in tumor cells. bioRxiv.

Yee D, Shah KM, Coles MC, Sharp TV, Lagos D, 2017. MicroRNA-155 induction via TNF-alpha and IFN-gamma suppresses expression of programmed death ligand-1 (PD-L1) in human primary cells. J Biol Chem 292, 20683–20693.

Zeisel A, Hochgerner H, Lonnerberg P, Johnsson A, Memic F, van der Zwan J, Haring M, Braun E, Borm LE, La Manno G, Codeluppi S, Furlan A, Lee K, Skene N, Harris KD, Hjerling-Leffler J, Arenas E, Ernfors P, Marklund U, Linnarsson S, 2018. Molecular Architecture of the Mouse Nervous System. Cell 174, 999–1014 e1022.

Zhang S, Edwards TN, Chaudhri VK, Wu J, Cohen JA, Hirai T, Rittenhouse N, Schmitz EG, Zhou PY, McNeil BD, Yang Y, Koerber HR, Sumpter TL, Poholek AC, Davis BM, Albers KM, Singh H, Kaplan DH, 2021. Nonpeptidergic neurons suppress mast cells via glutamate to maintain skin homeostasis. Cell.

Zhang XL, Lee KY, Priest BT, Belfer I, Gold MS, 2015. Inflammatory mediator-induced modulation of GABAA currents in human sensory neurons. Neuroscience 310, 401–409. [PubMed: 26415765]

Zheng Y, Yang W, Xia Y, Hawke D, Liu DX, Lu Z, 2011. Ras-induced and extracellular signal-regulated kinase 1 and 2 phosphorylation-dependent isomerization of protein tyrosine phosphatase (PTP)-PEST by PIN1 promotes FAK dephosphorylation by PTP-PEST. Mol Cell Biol 31, 4258–4269. [PubMed: 21876001]

Zhu W, Oxford GS, 2007. Phosphoinositide-3-kinase and mitogen activated protein kinase signaling pathways mediate acute NGF sensitization of TRPV1. Mol Cell Neurosci 34, 689–700. [PubMed: 17324588]

Zhu X, Lang J, 2017. Soluble PD-1 and PD-L1: predictive and prognostic significance in cancer. Oncotarget 8, 97671–97682.

Highlights

- PDL1, but not PD1, is widely expressed in murine and human sensory neurons.
- PD1 inhibits capsaicin-evoked behaviors and Ca^{2+} via reduction of membrane TRPV1.
- Anti-nociceptive effects of exogenous PD1 require neuronally expressed PDL1.

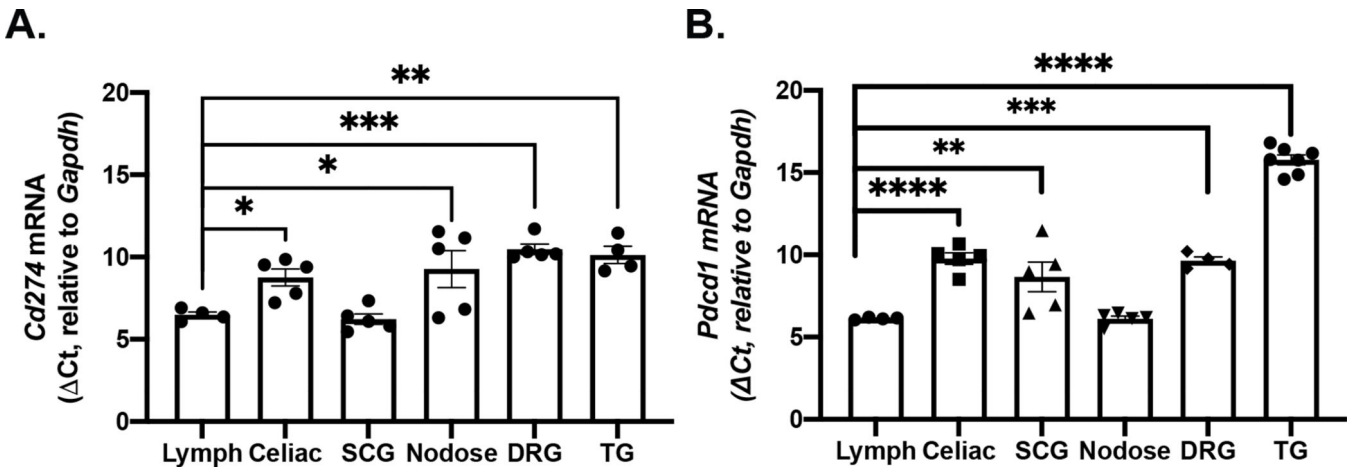

Figure 1. *Cd274* and *Pdcd1* mRNA expression in whole sensory and sympathetic ganglia.

(A) Plot shows relative level of *Cd274* mRNA detected in intact murine sympathetic and sensory ganglia and lymph nodes. Data were analyzed by one-way ANOVA, $F_{(5,18)}$=22.32, p<0.0001. Relative expression of *Cd274* in all sensory ganglia was significantly (p<0.05) lower than that in lymph nodes (Holm-Sidak's test). N=4–5/tissue. (B) Plot shows relative expression of *Pdcd1* mRNA in sympathetic and sensory ganglia and lymph nodes. Data were analyzed by one-way ANOVA and compared to lymph nodes, $F_{(5,20)}$=52.93, p<0.0001. The relative expression of *Pdcd1* in all ganglia except NG was significantly lower than that in lymph nodes (Holm-Sidak's test). N=4–7/tissue. SCG - superior cervical ganglia, NG - nodose ganglia, DRG - dorsal root ganglia, TG - trigeminal ganglia *p<0.05, **p<0.01, ***p<0.001, ****p<0.0001

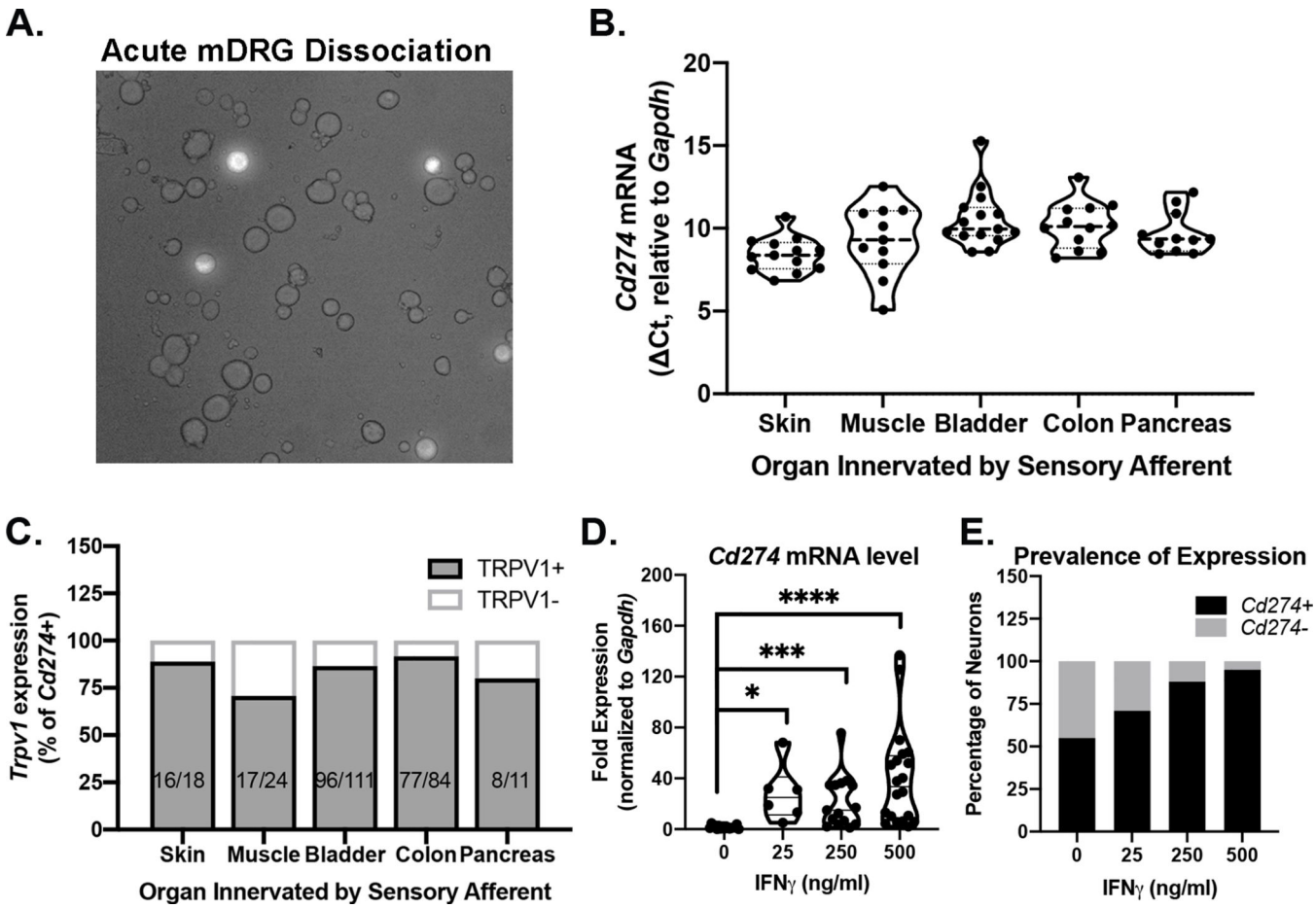

Figure 2. *Cd274* and *Pdcd1* mRNA expression in individual spinal sensory neurons.

mRNA analyses were conducted on individual retrogradely labeled sensory neurons collected following dissociation of DRG that innervate the targeted tissue (Panel A-C) or from dissociation of all DRG (Panel D,E). (A) Representative image of acutely dissociated mouse DRG revealing fluorescent labeling of colon afferents (20X). (B) *Cd274* mRNA, but not *Pdcd1* mRNA was detected in individual neurons innervating skin, muscle and visceral organs including colon, bladder, and pancreas. (C) *Trpv1* mRNA was detected in 70.8–91.7% of neurons in which *Cd274* mRNA was also detected. (D) DRG neurons incubated with IFNγ overnight show significantly increased levels *Cd274* mRNA expression. Fold expression was calculated using the ΔΔCt method. Neurons were collected from two independent experiments (Kruskal-Wallis Test followed by Dunn's post-hoc test, H=32.75, df=4, $p<0.001$). (E) IFNγ increases the proportion of neurons expressing detectable levels of *Cd274* mRNA. Data are pooled from two independent experiments (chi-square test $X^2_{(3, n=33)}=12.07$, $p=0.007$).

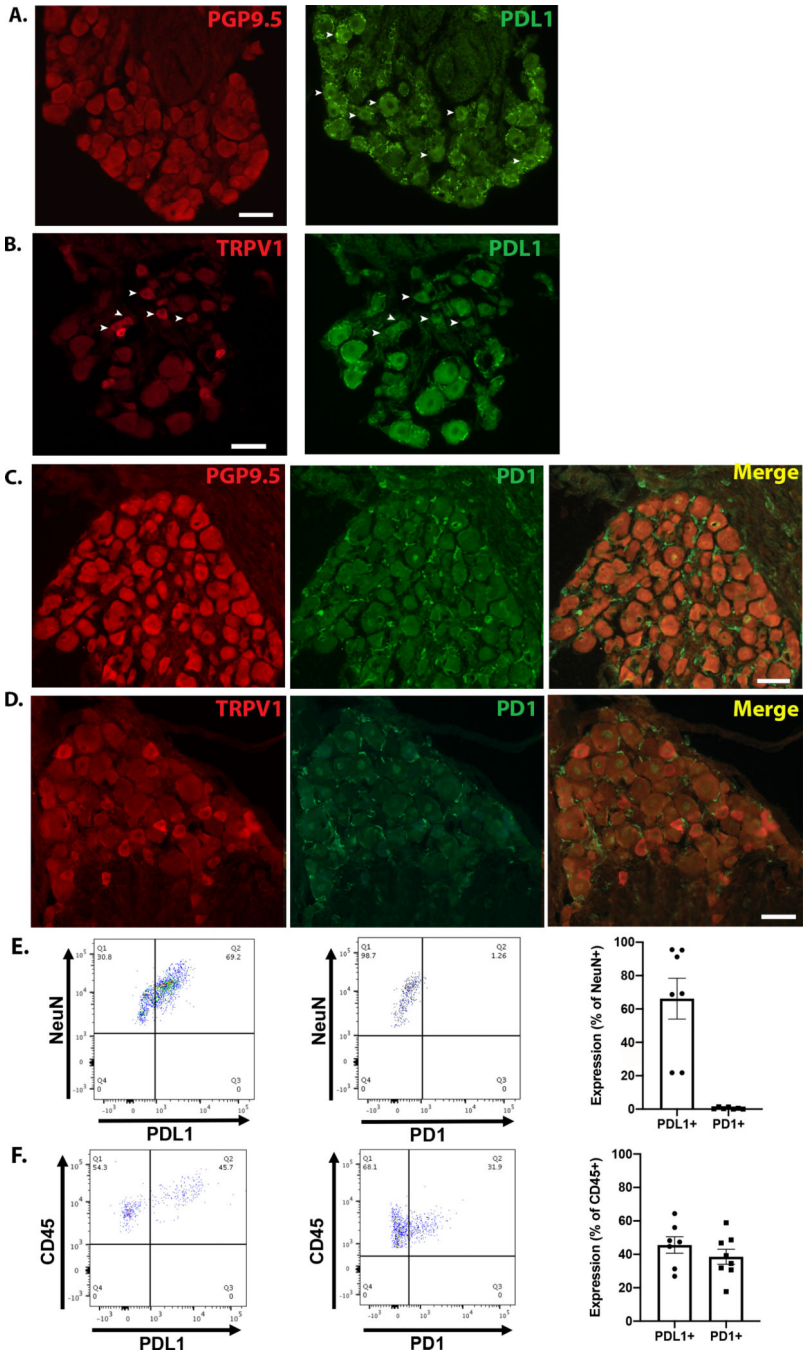

Figure 3. PDL1 and PD1 protein expression in mouse DRG.

(A) Mouse DRG were immunolabeled with the pan-neuronal marker PGP9.5 (left). After imaging the PGP9.5 staining, the same sections were subjected to a de-glycosylation reaction and subsequently immunolabeled for PDL1 (right). The arrowheads indicate PDL1 positive neurons. (B) Mouse DRG were immunolabeled for TRPV1 (left), followed by de-glycosylation and labeling for PDL1 (right). Arrowheads indicate co-localization of TRPV1 and PDL1. (C) DRG sections co-labeled for PGP9.5 (red) and PD1 (green) show no colocalization. (D) DRG sections were co-labeled for PD1 (green) and TRPV1 (red), but

no colocalization was observed. (C-D) Scale bars=50μm. Micrographs are representative of independent experiments performed on DRG from a minimum of 4 mice. (E) *left* Dot plot shows PDL1 expression in cells expressing the neuronal marker, NeuN. *middle* Dot plot shows negligible PD1 expression on DRG sensory neurons, marked by NeuN. *right* Group data indicate 66.2 ± 12.2% of DRG neurons express PDL1 while only 0.51 ± 0.2% of DRG neurons express PD1 protein. (F) *left* Representative dot plot showing PDL1 expression on non-neuronal (CD45+) cells isolated from mouse DRG. *middle* Representative dot plot shows PD1 expression on non-neuronal (CD45+) cells isolated from mouse DRG. *right* Group data show 45.6 ± 4.9% of CD45+ cells express PDL1 and 38.5 ± 4.5% express PD1. For flow cytometry experiments, N=7–8 per group.

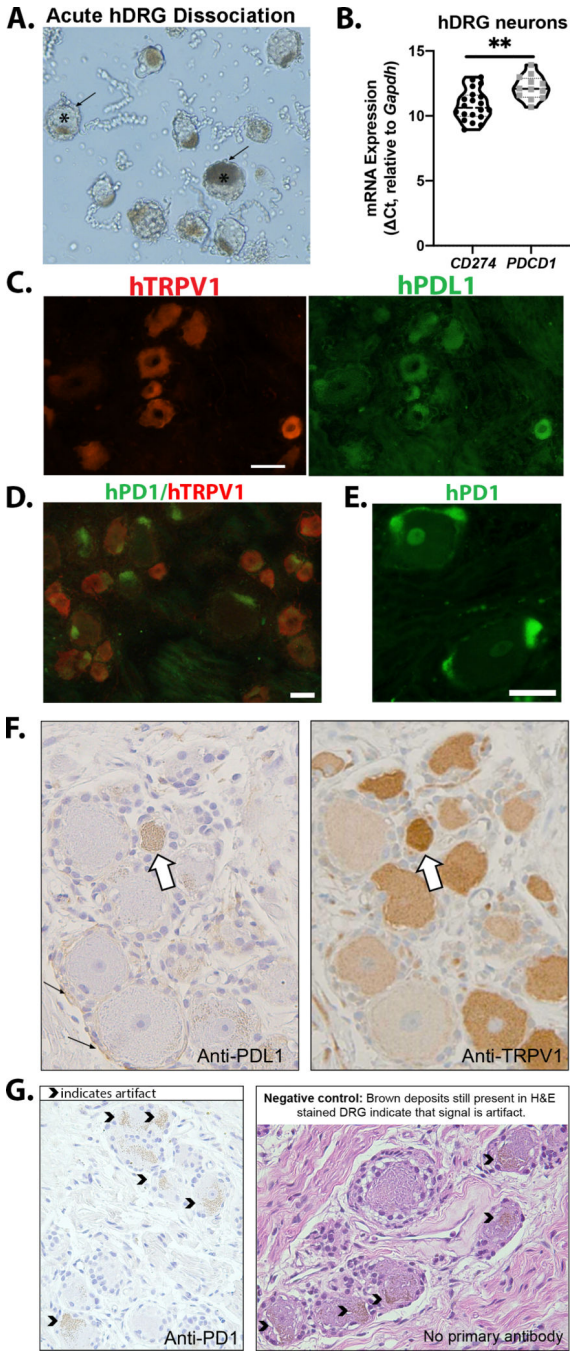

Figure 4. Expression of PDL1 and PD1 in human DRG neurons.

(A) Brightfield image of acutely dissociated human DRG (10X) used for collection of neurons for mRNA analysis. * marks examples of neurons surrounded by satellite glia (arrow). (B) *CD274* and *PDCD1* mRNA was detectable in human DRG neurons (n=24, N=3); *CD274* mRNA was significantly higher (lower ΔCt) compared to *PDCD1* mRNA, $t_{(30)}$=3.412, p=0.002 (Student's t test). (C) Representative micrographs of a human DRG section labeled to detect TRPV1, de-glycosylated and subsequently labeled for PDL1. (D) Representative micrograph of human DRG co-labeled with antibodies to TRPV1 and

PD1 (Biolegend). (E) High magnification (20X) image of human DRG labeled with anti-PD1 (Sigma) indicates expression in nonneuronal cells. Micrographs are representative of independent experiments performed on DRG from a minimum of 4 donors (Supplementary Table 1). (F) Adjacent sections of human DRG stained for PDL1 and TRPV1. White arrow indicates a neuron with expression of both PDL1 and TRPV1. Small black arrows indicate nonneuronal expression of PDL1. (G) PD1 immunoreactivity in human DRG was not detected via IHC. The caret symbols indicate brown signal that was determined to be artifact because it was also present in the negative controls (tissue sections in which primary antibody was excluded during the staining process). Detailed antibody information is provided in Supplementary Table 3 and 4. All scale bars=50μm.

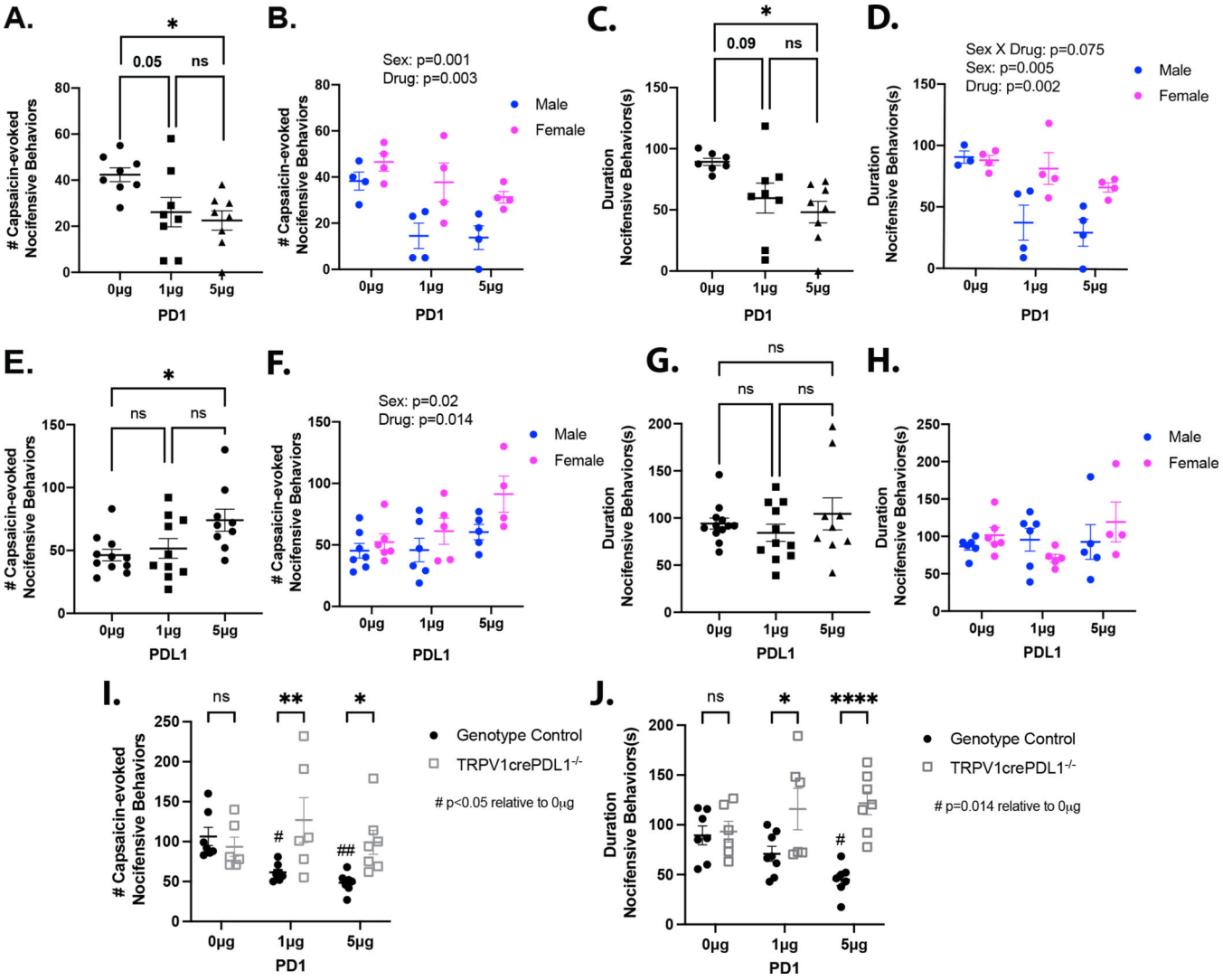

Figure 5. Neuronal PDL1 inhibits TRPV1-dependent pain-associated behavior.

(A) The number of capsaicin-evoked behaviors was significantly inhibited by exogenous PD1 (one-way ANOVA and Holm-Sidak's test, $F_{(2,21)}$=4.971, p=0.017). (B) There was a significant influence of sex on the impact of PD1 on the number of capsaicin-evoked behaviors (two-way ANOVA, Sex: $F_{(1,18)}$=14.723, p=0.001; Drug: $F_{(2,18)}$=8.244, p=0.003; Sex*Drug: $F_{(2,18)}$=1.054, p>0.05). (C) PD1 reduces the duration of capsaicin-evoked behaviors (one-way ANOVA and Holm-Sidak's test, $F_{(2,20)}$=5.064, p=0.017). One statistical outlier (determined by Grubbs' test) was excluded. (D) A statistical trend suggests that PD1 inhibits the duration of nocifensive behaviors specifically in male, but not female mice (two-way ANOVA followed by Holm-Sidak's test, Sex: $F_{(2,17)}$=10.30, p=0.005; Drug: $F_{(2,17)}$=8.719, p=0.004; Sex*Drug: $F_{(2,17)}$=3.02, p=0.075). (E) Exogenous PDL1 dose-dependently increased the number of capsaicin-evoked nocifensive behaviors (one-way ANOVA, $F_{(2,30)}$=3.999, p=0.029). (F) A two-way ANOVA revealed main effects of sex and drug on the number of capsaicin-evoked nocifensive behaviors following pretreatment with PDL1 (Sex: $F_{(1,27)}$=6.086, p=0.02; Drug: $F_{(2,27)}$=4.992, p=0.014). (G) PDL1 had no effect on the duration of capsaicin-evoked nocifensive behaviors (one-way ANOVA, $F_{(2,29)}$=0.844,

p>0.05). (H) The duration of capsaicin-evoked nocifensive behaviors following PDL1 treatment were not affected by sex (p>0.05). (I) PD1 had no effect on the number of capsaicin-evoked nocifensive behaviors in TRPV1cre:PDL1$^{fl/fl}$ mice (two-way ANOVA followed by Holm-Sidak's test, Genotype*Drug: $F_{(2,35)}$=4.489, p=0.018). (J) PD1 had no effect on the duration of capsaicin-evoked nocifensive behaviors in TRPV1cre:PDL1$^{fl/fl}$ mice (two-way ANOVA follow by Holm-Sidak's test, Genotype*Drug: $F_{(2,35)}$=5.22, p=0.01). N=6–12 per condition.

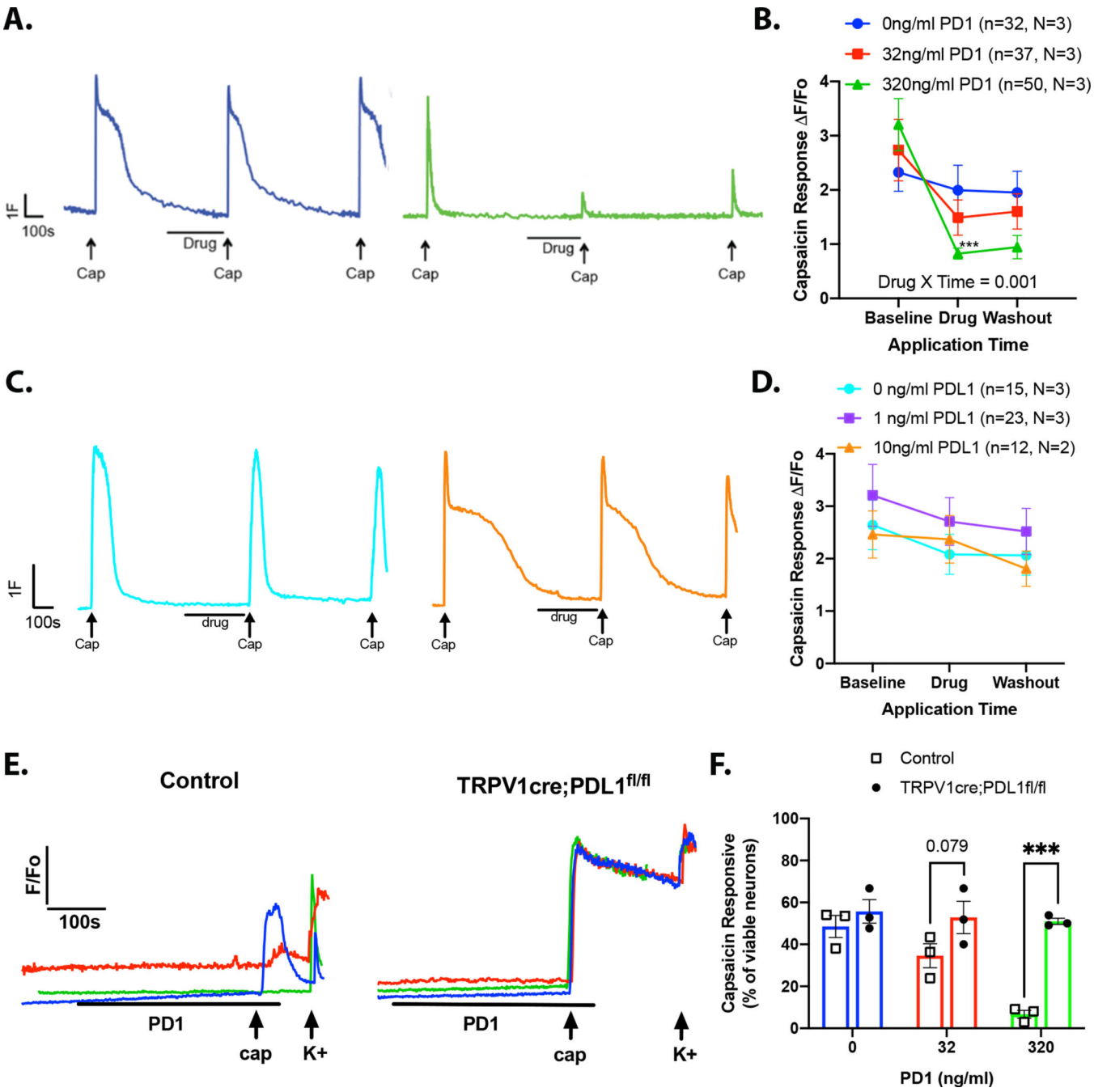

Figure 6. PDL1 intracellular signaling inhibits TRPV1-mediated calcium signaling.

(A-D) Capsaicin (300nM, 4s) was applied to DRG neurons three times with experimental drug applied for 5 min preceding the second capsaicin application. (A) Example traces from DRG neurons treated with vehicle (blue) or high dose PD1 (green). (B) Pooled data show that PD1 inhibits capsaicin responses in DRG neurons (two-way repeated measures ANOVA, Drug*Time: $F_{(4,232)}$=4.781, p=0.001). (C) Example traces from DRG neurons treated with vehicle (teal) or high dose PDL1 (orange). (D) PDL1 did not alter capsaicin responses in DRG neurons (two-way repeated measures ANOVA, Drug*Time:

F(4,70)=2.315, p>0.05). (E-F) PD1 (0, 32, or 320 ng/ml) was applied for 5 min prior to the application of capsaicin (300nM, 4s) to DRG cultures derived from TRPV1cre:PDL1$^{fl/fl}$ and littermate control mice. At the end of the experiment 50mM KCl was applied to identify viable cells. (E) Example traces of capsaicin evoked transients. (F) The proportion of capsaicin responders (relative to total viable neurons) was compared between neurons from genotype control and TRPV1cre:PDL1$^{fl/fl}$ (N=3, n=24–57 per mouse). PD1 dose-dependently reduced the proportion of capsaicin responders in control neurons only (two-way ANOVA followed by Sidak's test: genotype*drug: $F_{(2,12)}$=6.904, p=0.01).

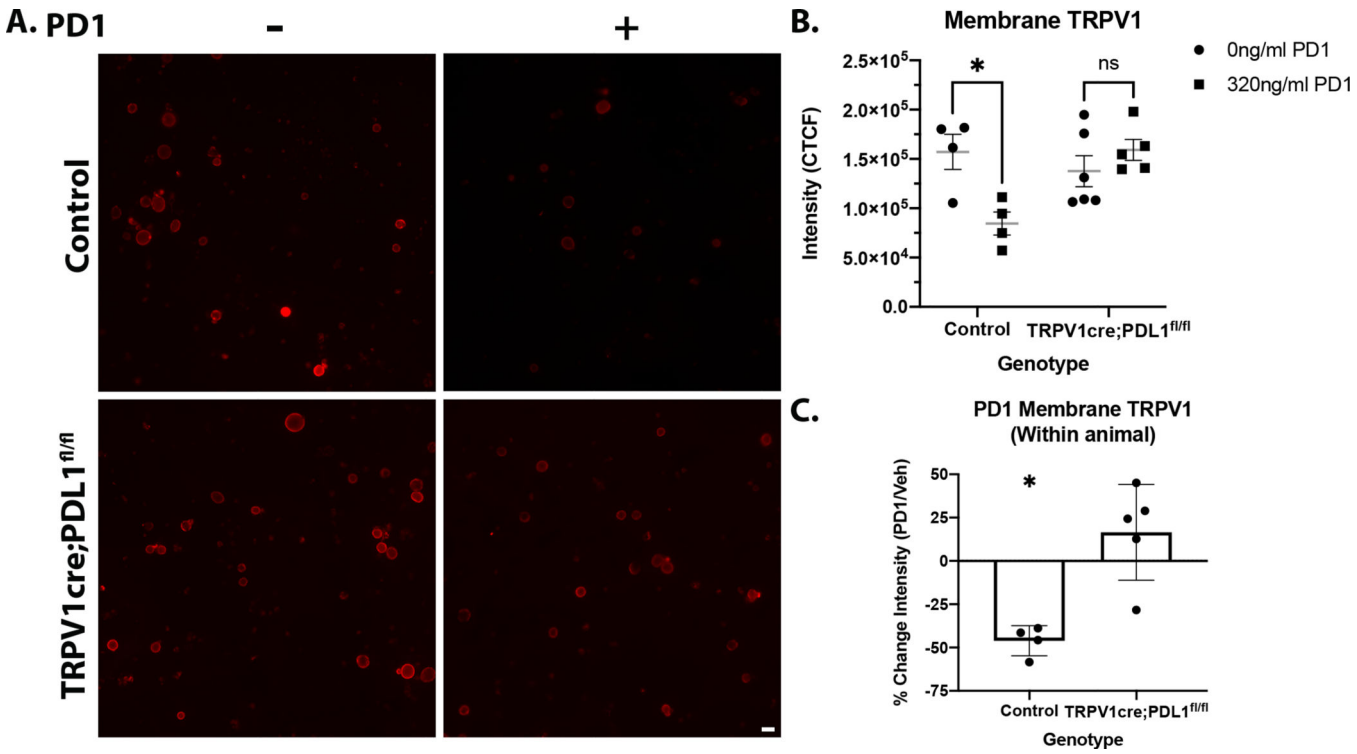

Figure 7. Engaging neuronal PDL1 decreases membrane TRPV1.

(A) Representative micrographs of membrane TRPV1 in DRG cultures from control and TRPV1cre:PDL1$^{fl/fl}$ mice that were treated with 0 or 320 ng/ml PD1. (B) Application of PD1 (320ng/ml) significantly reduced membrane TRPV1 in control neurons, but not PDL1 knockout neurons (two-way ANOVA followed by Holm Sidak's test: genotype*drug: $F_{(1,15)}$=10.15, p=0.006). (C) The percent change in TRPV1 signal of PD1-treated neurons relative to vehicle-treated neurons derived from the same mouse illustrates that PD1 significantly reduces membrane TRPV1 in control, but not PDL1 knockout neurons ($t_{(7)}$=3.208, p=0.004). N=4–5 per genotype